European Journal of Radiology Open 9 (2022) 100403

Contents lists available at ScienceDirect

European Journal of Radiology Open

journal homepage: www.elsevier.com/locate/ejro

Synthetic magnetic resonance imaging for primary prostate cancer evaluation: Diagnostic potential of a non-contrast-enhanced bi-parametric approach enhanced with relaxometry measurements

Yuki Arita [a], Hirotaka Akita [a], Hirokazu Fujiwara [a], Masahiro Hashimoto [a], Keisuke Shigeta [b], Thomas C. Kwee [c], Soichiro Yoshida [d], Takeo Kosaka [b], Shigeo Okuda [a], Mototsugu Oya [b], Masahiro Jinzaki [a,*]

[a] Department of Radiology, Keio University School of Medicine, 35 Shinanomachi, Shinjuku-ku, Tokyo 160-8582, Japan
[b] Department of Urology, Keio University School of Medicine, 35 Shinanomachi, Shinjuku-ku, Tokyo 160-8582, Japan
[c] Department of Radiology, Nuclear Medicine, and Molecular Imaging, University Medical Center Groningen, Hanzeplein 1, PO Box 30.001, 9700 RB Groningen, The Netherlands
[d] Department of Urology, Tokyo Medical and Dental University Graduate School, 1-5-45 Yushima, Bunkyo-ku, Tokyo 113-8519, Japan

HIGHLIGHTS

- Diagnostic performances of synthetic bpMRI and conventional bpMRI are comparable for primary PCa
- Diagnostic performance of synthetic MRI variables are similar to that of DCE-MRI for csPCa in PZ
- Synthetic bpMRI shows potential as a contrast agent-free method for primary PCa

ARTICLE INFO

Keywords:
Primary prostate cancer
Magnetic resonance imaging
Multiparametric Magnetic Resonance Imaging
Contrast agents
Biomarkers

ABSTRACT

Purpose: Bi-parametric magnetic resonance imaging (bpMRI) with diffusion-weighted images has wide utility in diagnosing clinically significant prostate cancer (csPCa). However, bpMRI yields more false-negatives for PI-RADS category 3 lesions than multiparametric (mp)MRI with dynamic-contrast-enhanced (DCE)-MRI. We investigated the utility of synthetic MRI with relaxometry maps for bpMRI-based diagnosis of csPCa.
Methods: One hundred and five treatment-naïve patients who underwent mpMRI and synthetic MRI before prostate biopsy for suspected PCa between August 2019 and December 2020 were prospectively included. Three experts and three basic prostate radiologists evaluated the diagnostic performance of conventional bpMRI and synthetic bpMRI for csPCa. PI-RADS version 2.1 category 3 lesions were identified by consensus, and relaxometry measurements (T1-value, T2-value, and proton density [PD]) were performed. The diagnostic performance of relaxometry measurements for PI-RADS category 3 lesions in peripheral zone was compared with that of DCE-MRI. Histopathological evaluation results were used as the reference standard. Statistical analysis was performed using the areas under the receiver operating characteristic curve (AUC) and McNemar test.
Results: In 102 patients without significant MRI artefacts, the diagnostic performance of conventional bpMRI was not significantly different from that of synthetic bpMRI for all readers ($p = 0.11–0.79$). The AUCs of the combination of T1-value, T2-value, and PD (T1 + T2 + PD) for csPCa in peripheral zone for PI-RADS category 3

Abbreviations: ADC, apparent diffusion coefficient; BpMRI, Bi-parametric magnetic resonance imaging; csPCa, clinically significant PCa; DCE-MRI, dynamic contrast-enhanced MRI; DWI, diffusion-weighted imaging; ISUP, International Society of Urological Pathology; MpMRI, Multiparametric MRI; MRI, magnetic resonance imaging; PCa, prostate cancer; PD, proton density; PI-RADS v2.1, Prostate Imaging Reporting and Data System version 2.1; PZ, peripheral zone; ROI, region of interest; TE, echo time; TR, repetition time; TZ, transition zone; T2WI, T2-weighted imaging.

* Corresponding author.
E-mail addresses: yarita@rad.med.keio.ac.jp (Y. Arita), hakita@rad.med.keio.ac.jp (H. Akita), hfujiwar@rad.med.keio.ac.jp (H. Fujiwara), m.hashimoto@rad.med.keio.ac.jp (M. Hashimoto), keisukeshigeta@yahoo.co.jp (K. Shigeta), thomaskwee@gmail.com (T.C. Kwee), 6030uro@tmd.ac.jp (S. Yoshida), takemduro@gmail.com (T. Kosaka), okuda@rad.med.keio.ac.jp (S. Okuda), moto-oya@z3.keio.jp (M. Oya), jinzaki@rad.med.keio.ac.jp (M. Jinzaki).

https://doi.org/10.1016/j.ejro.2022.100403
Received 14 January 2022; Accepted 9 February 2022

lesions were 0.85 for expert and 0.86 for basic radiologists, with no significant difference between T1 + T2 + PD and DCE-MRI for both expert and basic radiologists (p = 0.29–0.45).
Conclusion: Synthetic MRI with relaxometry maps shows promise for contrast media-free evaluation of csPCa.

1. Introduction

Prostate cancer (PCa) is the most common cancer and the second leading cause of cancer-related deaths in men [1]. Although the life expectancy for localised PCa has markedly increased over the past few decades, distinguishing clinically significant PCa (csPCa) by imaging is challenging due to the multi-focal nature of the disease [2,3]. Magnetic resonance imaging (MRI) has been widely applied for PCa detection [4,5], and multiparametric MRI (mpMRI) (a combination of T2-weighted imaging [T2WI], diffusion-weighted imaging [DWI], and dynamic contrast-enhanced MRI [DCE-MRI]) has been established for csPCa detection and prediction of patient outcomes [6,7]. The important role of mpMRI has also been acknowledged in the Prostate Imaging and Reporting and Data System version 2.1 (PI-RADS v2.1) [8,9]. DWI has been used as an essential functional sequence for peripheral zone (PZ) PCa, while T2WI is considered the leading sequence for transition zone (TZ) PCa. For the PZ, if the DCE-MRI findings meet the criteria, lesions in category 3 can be reclassified to category 4 [8,9].

Recently, bi-parametric (bp) MRI (a combination of T2WI and DWI) has been proposed as an alternative to mpMRI with gadolinium-enhanced sequences, reducing the costs and potential side effects of gadolinium-based contrast agents [9–11]. According to a meta-analysis based on the PI-RADS v2 criteria, both methods achieve a comparable diagnostic performance for csPCa [12]. However, recent studies have indicated that the diagnostic performance of bpMRI is inferior to that of mpMRI when interpreted by non-expert radiologists [13,14]; moreover, the sensitivity of bpMRI for csPCa is lower than that of mpMRI when the PI-RADS v2.1 system is used, particularly for category 3 lesions [9,15]. Therefore, when evaluating csPCa without contrast media in bpMRI, the arising challenge is to improve the diagnostic accuracy of lesions that are determined to be category 3 in bpMRI but would be reclassified to category 4 when relying on DCE-MRI findings in an mpMRI protocol.

Synthetic MRI is an emerging technique that synthesises MR images at arbitrary contrast after the actual MR acquisition, which may allow for the quantitative assessment of lesions without contrast media [16–20]. In a recent study, Cui, et al. revealed that the diagnostic performance of relaxometry maps [T1-value, T2-value, and proton density (PD)] was inferior to that of the apparent diffusion coefficient (ADC) values for discriminating between PCa and other benign entities [21]. However, comparison of the diagnostic performances between relaxometry maps and DCE-MRI-based PI-RADS scores remains unknown.

The purpose of this study was to investigate the utility of synthetic MRI for bpMRI evaluation of primary PCa by assessing the impact of the reader's experience (expert or basic prostate radiologists) on the bpMRI-based diagnostic performance and comparing the diagnostic performance of relaxometry maps derived from synthetic MRI with that of DCE-MRI for category 3 lesions in PZ.

2. Materials and methods

This prospective study was approved by the medical ethics committee of our institution (approval number: 20190148), and written informed consent was obtained from all patients included.

2.1. Patients

One hundred and five treatment-naïve patients suspected to have PCa based on an elevated serum prostate-specific antigen level or abnormal digital rectal examination, who underwent conventional prostate mpMRI, including T2WI, DWI, and DCE-MRI, prior to MRI-ultrasonography fusion-guided prostate-targeted biopsy (MRGB) between August 2019 and December 2020, were prospectively included in this study. All patients also underwent synthetic MRI at the time of conventional prostate mpMRI. Patients whose MRI scans were degraded due to prominent susceptibility artefacts from previous hip replacement (n = 3) were excluded. The remaining 102 patients were eligible for analysis (Fig. 1).

2.2. Image acquisition

Conventional prostate mpMRI and synthetic MRI were acquired using a 3.0-T system (DISCOVERY MR750 • SIGNA Pioneer; GE Healthcare, WI, USA) (Fig. 2). The parameters for DWI comprised: repetition time (TR)/echo time (TE), 4500/55.3 ms; and two different b-values (50 and 800 s/mm^2). Computed intermediate and high b-value DWI (1000, 1500, and 2000 s/mm^2) and ADC maps were generated from the native DWI dataset (i.e., 50 and 800 s/mm^2) on the MR console. The parameters used for T2WI comprised: TR/TE, 6000/120 ms; DCE-MRI: TR/TE, 4/1.1, 2.2 ms. Data acquisition for DCE-MRI began simultaneously with the start of intravenous injection of a gadolinium-based contrast medium at 0.1 mmol/kg of gadobutrol (Gadovist, Bayer Schering Pharma) at a rate of 1.5 mL/s via power injector, followed by a 30-mL saline flush at the same rate as contrast medium injection. Multiphase DCE-MR images were obtained every 7 s for 210 s (30 phases). The parameters for synthetic MRI comprised: TR/TE, 4500/13.6, 88.5 ms [16]. Synthetic T2WI was generated for TR/TE, 6000/100 ms on the MR console prior to the reading evaluation. The sequence parameters used for conventional mpMRI and synthetic MRI are shown in Supplementary Table 1.

2.3. Image analysis

2.3.1. Subjective assessment of image quality

Two bpMRI datasets were sent to our institutional imaging server system for review:

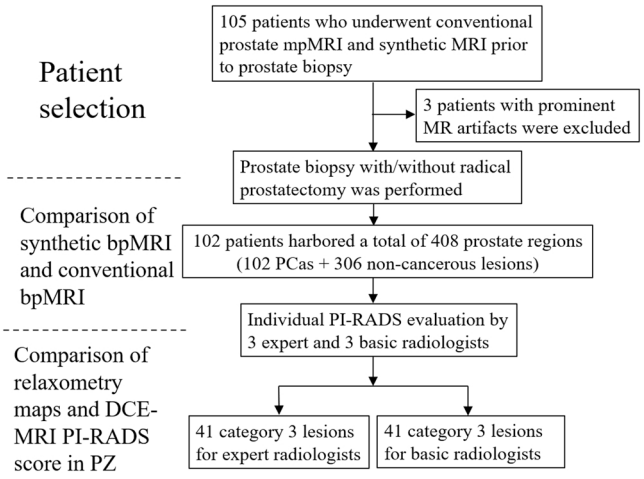

Fig. 1. Patient selection flowchart. Abbreviations: MRI: magnetic resonance imaging; mpMRI: multiparametric MRI; bpMRI: bi-parametric MRI; DCE: dynamic contrast-enhanced; PI-RADS: Prostate Imaging Reporting and Data System; PZ: peripheral zone.

(a) Conventional bpMRI: axial DWI scans with a b-value of 2000 s/mm^2 + axial conventional T2WI scans, and
(b) Synthetic bpMRI: axial DWI scans with a b-value of 2000 s/mm^2 + axial synthetic T2WI scans.

Both bpMRI datasets were reviewed along with the ADC maps for reference, using a multimodality workstation (Centricity™ Universal Viewer, PACS, GE Healthcare, WI, USA). The reviewers were blinded to the type of sequence and parameters under evaluation. The two bpMRI datasets were independently evaluated by six radiologists (three experts who had performed prostate MR evaluations in >1000 cases and three basic prostate radiologists who had performed prostate MR evaluations in >400 cases based on the criteria of the ESUR/ESUI consensus statements) [13], who were blinded to all clinical and pathological data, including any previous imaging data. The two bpMRI datasets of each patient were assigned anonymous identifiers and reviewed in a random order [22,23]. For each reader, there was at least a 1-month interval between reading pairs of images (i.e., Conventional bpMRI and Synthetic bpMRI) to avoid recall bias.

While reviewing each T2WI scan (synthetic T2WI and conventional T2WI), all six readers subjectively evaluated each image on a scale of 1–5 (with a score of 1 corresponding to the worst quality and a score of 5 corresponding to the highest quality) for the following items: contraction artefacts (i.e., artefacts resulting from bowel peristalsis and contraction of the urinary bladder), motion artefacts (i.e., breathing and patient movement), and overall image quality (the image quality was evaluated per T2W-series) [24,25].

2.4. PI-RADS scoring evaluation

For each of the four prostate regions, i.e., right and left TZ, and right and left PZ, DWI, and T2WI scans of each bpMRI dataset were scored using a five-point scoring system, with DWI as the dominant sequence for the PZ and T2WI for the TZ, to obtain an overall score according to the PI-RADS v2.1 criterion [9]. A PI-RADS score between 1 (low likelihood) and 5 (high likelihood) was assigned to denote csPCa (International Society of Urological Pathology (ISUP) grade group ≥ 2 tumours) [9]. When multiple tumours were present in one prostate region (i.e., right and left TZ, and right and left PZ), the tumour with the highest score (index lesion) was used to calculate the score for that prostate region.

2.5. Comparison between relaxometry maps derived from synthetic MRI and DCE-MRI PI-RADS scores for category 3 lesions in PZ

Subsequently, three expert prostate radiologists and three basic prostate radiologists each identified all PI-RADS category 3 lesions on synthetic bpMRI in the PZ by consensus and placed a region of interest (ROI) on the lesion to measure the relaxometry values of the lesion. Dedicated analysis software for synthetic MRI automatically calculated the relaxometry values. The mean T1, T2, and PD values of the pixels within the ROI were used as relaxometry measurements for further analyses. For groupwise comparisons, the mean of the values measured by each of the three readers was used for statistical analysis [26]. The PD level of pure water was set at 100%.

At the time of relaxometry map analyses, the DCE-MRI PI-RADS score (positive/negative) was determined by both expert and basic radiologists in each case by consensus based on the PI-RADS v2.1 criteria [9]. Lesions featuring focal enhancements occurring earlier or concurrent to the enhancement of contiguous normal prostate tissue, which generally corresponds to a suspicious finding in T2WI and/or DWI, were assigned a positive DCE-MRI PI-RADS score [9].

2.6. Reference standard

The radical prostatectomy specimen was selected as the final

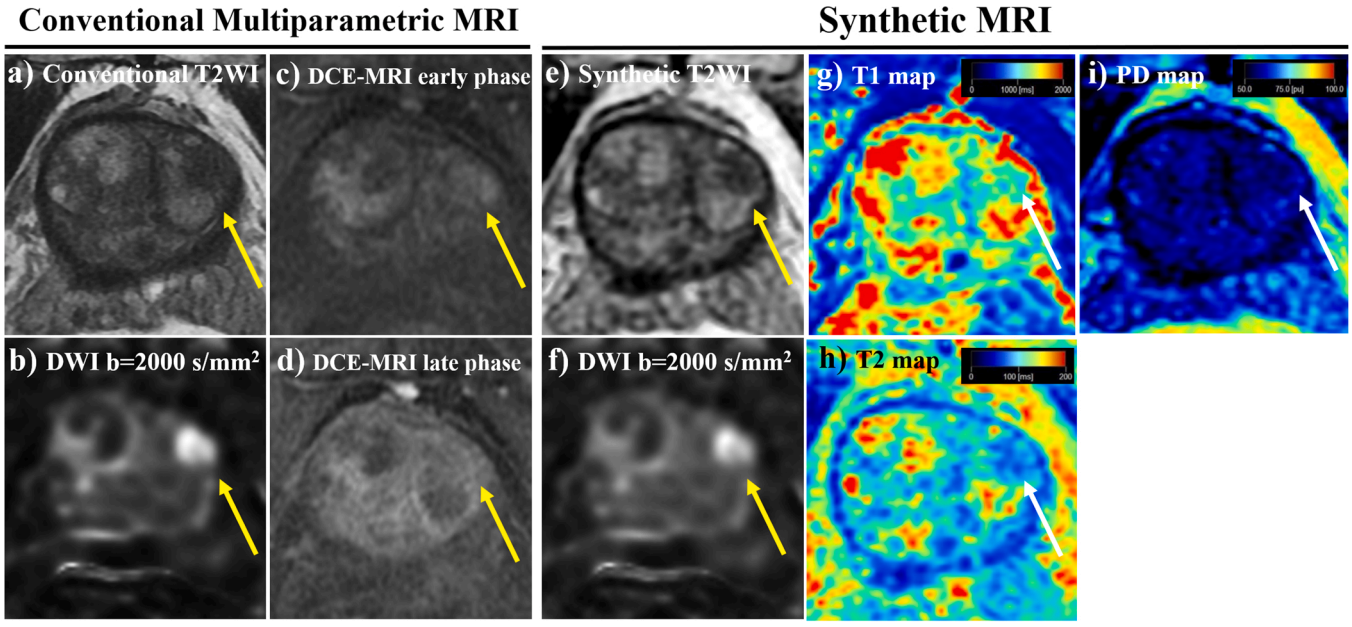

Fig. 2. A representative case: a 68-year-old man with a 12-mm PCa in the left TZ (adenocarcinoma cT2a, ISUP grade group 2, PSA 8.6 ng/mL). (**a**) Axial conventional and (**e**) synthetic T2WI scans both equivalently show a low-signal intensity focus in normal-appearing prostate tissue in the left TZ (arrow). (**b**) Axial conventional and (**f**) synthetic DWI scans with a b-value of 2000 s/mm^2 demonstrate a high-signal intensity focus corresponding to the location of the abnormal signal on the T2WI scan (arrow) (**c**), (**d**) Axial DCE-MRI scans show focal enhancement, which precedes the enhancement of adjacent normal prostatic tissue, corresponding to the location of the abnormal signal on the T2WI and DWI scans (thus, translating to a positive DCE-MRI PI-RADS score) (arrow). (**g**) Axial T1, (**h**) T2, and (**i**) PD maps were generated using a dedicated synthetic MRI analysis software; the corresponding lesion T1-value, T2-value, and PD were 1173 ms, 83.0 ms, and 66.0%, respectively. Abbreviations: PCa: prostate cancer; TZ: transition zone; ISUP: International Society of Urological Pathology; PSA: prostate-specific antigen; T2WI: T2-weighted imaging; DWI: diffusion-weighted imaging; PI-RADS: Prostate Imaging Reporting and Data System; DCE: dynamic contrast-enhanced; PD: proton density.

pathological reference standard for determining the absence or presence of PCa in each of the four regions of the prostate in patients who underwent MRGB and subsequent radical prostatectomy. MRGB was used as the reference standard for the remaining patients [15, 21–23, 27, 28]. All MRGB procedures were performed using the UroStation system (Koelis; Grenoble, France) with elastic image fusion, real-time 3-dimensional organ-tracking technology, and a computer workstation (Koelis) for segmentation of the prostate and the lesion under local perianal muscle and transrectal ultrasonography-guided periprostatic plexus anesthesia [27]. The pathologically dominant lesion was defined as the one with the highest-grade group or the largest size (in case of equal grade grouping) for each side in the PZ and TZ. Grade groups were assigned according to the 2019 ISUP consensus conference guidelines. ISUP grade group $\geq$ 2 tumours were considered csPCa [9].

2.7. Statistical analysis

Exact Wilcoxon signed-rank tests were used to compare the conventional and synthetic T2WI scans with respect to the readers' assessment on image quality. Interobserver agreement of PI-RADS v 2.1 overall score among all six radiologists for conventional and synthetic bpMRI, respectively, was assessed by Fleiss' kappa statistic. Receiver operating characteristic (ROC) curve analysis based on logistic regression was performed to assess the diagnostic performance of the conventional and synthetic bpMRI datasets for a csPCa on a regional basis. The optimal cut-off value was determined by the Youden-index. The areas under the curve (AUCs) were compared using the Z-test. The sensitivity and specificity of the two bpMRI datasets for csPCa on a regional basis (cut-off PI-RADS score $\geq$3) were compared using the McNemar test. For PI-RADS category 3 lesions in the PZ, the interobserver agreement of relaxometry measurements among six radiologists was assessed with the Fleiss' kappa statistic. Differences in relaxometry measurements between csPCa and other entities (i.e. clinically insignificant PCa, and non-cancerous lesions) were compared with the Wilcoxon rank sum test. ROC curve analysis based on univariable or multivariable logistic regression was performed to assess the diagnostic performance of the combination of T1-value, T2-value, and PD for csPCa in category 3 lesions [29]. The optimal cut-off value was determined by the Youden-index. The AUCs were compared using the Z-test. The sensitivity and specificity between synthetic MRI-derived relaxometry measurements and the DCE-MRI PI-RADS score for csPCa were compared using the McNemar test. All *p*-values were two-sided and *p*-values < 0.05 were considered statistically significant. ROC curve analysis was performed using IBM SPSS Statistics v20 (IBM Corp., Armonk, NY, USA). Other statistical analyses were performed using SAS software v9.4 (SAS Institute, Cary, NC, USA).

3. Theory/calculation

3.1. Theory

MpMRI has been widely employed for PCa evaluation, particularly for the diagnosis of csPCa prior to prostate biopsy; however, it has some disadvantages, including high costs and potential side effects from gadolinium-based contrast agents [9–11]. Recently, bpMRI has been proposed as an alternative to mpMRI with gadolinium-enhanced sequences [12]. Similarly, the need for reducing false-negatives in PI-RADS category 3 lesions and improving the assessment of category 3 lesions without contrast administration remain important challenges [9, 13–15].

3.2. Calculation

Synthetic MRI would be beneficial as a non-contrast-enhanced protocol for the diagnosis of csPCa, if the diagnostic performance of synthetic bpMRI was comparable to that of conventional bpMRI and its relaxometry maps, which may represent the signature of csPCa [20,21], and provide a diagnostic performance similar to the DCE-MRI-based PI-RADS score for category 3 lesions in PZ.

4. Results

4.1. Patients' and PCa lesions' characteristics

The clinicopathological data are shown in Table 1. The median time between MRI and subsequent prostate biopsies was 4 weeks (range, 1–6 weeks). All 102 included patients received MRGB. A total of 52 patients were diagnosed with PCa, and the number of regions diagnosed with PCa was 1/2/3/4 in 18/22/8/4 patients. Among the 52 PCa patients, 37 underwent radical prostatectomy.

PCa was present in 102 regions (59/43 in TZ/PZ) out of a total of 408 regions (204/204 in TZ/PZ); ISUP grade group 1 (n = 8/6), grade group 2 (n = 22/16), grade group 3 (n = 16/11), grade group 4 (n = 11/9), and grade group 5 (n = 2/1). The non-cancerous lesions (n = 145/161) consisted of benign prostate hyperplasia, prostatitis, and normal TZ or PZ.

4.2. Comparison of the subjective image quality scores

The subjective image quality grading (average score) of each T2WI dataset (conventional vs. synthetic) of the 102 included patients is shown in Supplementary Table 2. No significant difference was observed between the two datasets regarding contraction artefacts, motion artefacts and overall image quality for both TZ and PZ, for all the six readers (p = 0.27–0.81). Representative cases of subjective scores of overall image quality are shown in Supplementary Fig. 1.

4.3. Comparison of the conventional and synthetic bpMRI datasets for primary PCa evaluation according to the PI-RADS criteria

The diagnostic performance of the two bpMRI datasets for csPCa is shown in Table 2. The Fleiss' kappa values for interobserver agreement regarding PI-RADS v 2.1 overall score among all six radiologists were 0.76 and 0.79 for the TZ and PZ, respectively, in conventional bpMRI, and 0.75 and 0.78 for the TZ and PZ, respectively, in synthetic bpMRI. The Fleiss' kappa values for interobserver agreements regarding PI-RADS v 2.1 overall score among expert/basic prostate radiologists were 0.82/0.78 and 0.80/0.78 for the TZ and PZ, respectively in conventional bpMRI, and 0.79/0.78 and 0.83/0.82 for the TZ and PZ, respectively, in synthetic bpMRI.

For the TZ, the AUCs for the diagnosis of csPCa using conventional bpMRI/synthetic bpMRI evaluated by expert prostate radiologists 1, 2,

Table 1
Characteristics of the patients (n = 52) and their index PCa lesions (n = 102).

Patient characteristics	
Age, years	67.7 (44–85)[a]
PSA level, ng/mL	7.82 (4.25–18.3)[a]
Prostate cancer characteristics	
Clinical stage (T1c/T2a/T2b/T2c/T3a/T3b)	2 (3.9)/29 (55.8)/5 (9.6)/10 (19.2)/5 (9.6)/1 (1.9)[b]
Site of the index lesion (Tr. TZ/Lt. TZ/Rt. PZ/Lt. PZ)	29 (28.4)/30 (29.4)/22 (21.6)/21 (20.6)[b]
Maximum lesion length, mm (TZ/PZ)	7.4 (0–25.7)/ 7.1 (0–22.9)[a]
Dominant lesion Gleason score (TZ/PZ)	
6	8 (13.6)/ 6 (14.0)[b]
7	38 (64.4)/ 27 (62.8)[b]
8–10	13 (22.0)/ 10 (23.2)[b]

PCa: prostate cancer; PSA: prostate-specific antigen; Rt: right; Lt: left; TZ: transition zone; PZ: peripheral zone

[a] Data presented in terms of the median (range)

[b] Data presented in terms of the number (percentage)

Table 2
Comparison of the diagnostic performance of the two bpMRI datasets for csPCa using a cutoff score of ≥ 3 according to the PI-RADS version 2.1.

Prostate Radiologist	Region	Parameter	Reader	Conventional bpMRI	Synthetic bpMRI	*p*-value
Expert	TZ	Sensitivity, %	1	92.2 (47/51)	88.2 (45/51)	0.16
			2	90.2 (46/51)	88.2 (45/51)	0.56
			3	88.2 (45/51)	90.2 (46/51)	0.56
		Specificity, %	1	83.7 (128/153)	86.3 (132/153)	0.16
			2	87.6 (134/153)	86.3 (132/153)	0.53
			3	84.3 (129/153)	85.6 (131/153)	0.59
		Positive predictive values, %	1	65.3 (47/72)	68.2 (45/66)	0.35
			2	70.8 (46/65)	68.2 (45/66)	0.42
			3	65.2 (45/69)	67.6 (46/68)	0.45
		Negative predictive values, %	1	97.0 (128/132)	95.7 (132/138)	0.55
			2	96.4 (134/139)	95.7 (132/138)	0.68
			3	95.6 (129/135)	96.3 (131/136)	0.66
	PZ	Sensitivity, %	1	83.8 (31/37)	81.1 (30/37)	0.32
			2	81.1 (30/37)	78.4 (29/37)	0.35
			3	81.1 (30/37)	75.7 (28/37)	0.16
		Specificity, %	1	88.0 (147/167)	86.8 (145/167)	0.48
			2	90.4 (151/167)	87.4 (146/167)	0.20
			3	88.0 (147/167)	86.8 (145/167)	0.48
		Positive predictive values, %	1	60.8 (31/51)	57.7 (30/52)	0.36
			2	65.2 (30/46)	58.0 (29/50)	0.14
			3	60.0 (30/50)	56.0 (28/50)	0.32
		Negative predictive values, %	1	96.1 (147/153)	95.4 (145/152)	0.65
			2	95.6 (151/158)	94.8 (146/154)	0.68
			3	95.5 (147/154)	94.2 (145/154)	0.50
Basic	TZ	Sensitivity, %	1	84.3 (43/51)	82.4 (42/51)	0.64
			2	82.4 (42/51)	80.4 (41/51)	0.35
			3	84.3 (43/51)	80.4 (41/51)	0.16
		Specificity, %	1	79.7 (122/153)	76.5 (117/153)	0.39
			2	78.4 (120/153)	76.5 (117/153)	0.26
			3	76.5 (117/153)	75.8 (116/153)	0.76
		Positive predictive values, %	1	58.1 (43/74)	53.8 (42/78)	0.35
			2	56.0 (42/75)	53.2 (41/77)	0.45
			3	54.4 (43/79)	52.6 (41/78)	0.53
		Negative predictive values, %	1	93.8 (122/130)	92.9 (117/126)	0.65
			2	93.0 (120/129)	92.1 (117/127)	0.65
			3	93.6 (117/125)	92.1 (116/126)	0.58
	PZ	Sensitivity, %	1	81.1 (30/37)	75.7 (28/37)	0.16
			2	81.1 (30/37)	75.7 (28/37)	0.16
			3	75.7 (28/37)	73.0 (27/37)	0.56
		Specificity, %	1	81.4 (136/167)	85.0 (142/167)	0.11
			2	86.2 (144/167)	84.4 (141/167)	0.32
			3	85.0 (142/167)	84.4 (141/167)	0.78
		Positive predictive values, %	1	49.2 (30/61)	52.8 (28/53)	0.35
			2	56.6 (30/53)	51.9 (28/54)	0.25
			3	52.8 (28/53)	50.9 (27/53)	0.50
		Negative predictive values, %	1	95.1 (136/143)	94.0 (142/151)	0.65
			2	95.4 (144/151)	94.0 (141/150)	0.58
			3	94.0 (142/151)	93.4 (141/151)	0.70

bpMRI: bi-parametric magnetic resonance imaging; csPCa: clinically significant prostate cancer; PI-RADS: Prostate Imaging Reporting and Data System; TZ: transition zone; PZ: peripheral zone; Conventional bpMRI: axial diffusion-weighted imaging (DWI) scans with a b-value of 2000 s/mm2 + pre-biopsy pelvic axial conventional T2-weighted imaging (T2WI) scans; Synthetic bpMRI: axial DWI scans with a b-value of 2000 s/mm2 + synthetic T2WI scans
* $p < 0.05$, statistically significant

and 3 were 0.93/0.92, 0.93/0.92, and 0.92/0.93, respectively, and there was no significant difference in the diagnostic performance between conventional bpMRI and synthetic bpMRI for all readers (p = 0.25, 0.27, and 0.79, for each reader). The AUCs for the diagnosis of csPCa using conventional bpMRI/synthetic bpMRI evaluated by basic prostate radiologists 1, 2, and 3 were 0.89/0.88, 0/88/0.87, and 0.88/0.86, respectively, and there was no significant difference in diagnostic performance between conventional bpMRI and synthetic bpMRI for all readers (p = 0.29, 0.32, and 0.14, for each reader). For the PZ, the AUCs for the diagnosis of csPCa using conventional bpMRI/synthetic bpMRI evaluated by expert prostate radiologists 1, 2, and 3 were 0.93/0.91, 0.91/0.89, and 0.90/0.88, respectively, and there was no significant difference in diagnostic performance between conventional bpMRI and synthetic bpMRI for all readers (p = 0.16, 0.59, and 0.11, for each reader). The AUCs for the diagnosis of csPCa using conventional bpMRI/synthetic bpMRI evaluated by basic prostate radiologists 1, 2, and 3 were 0.91/0.88, 0.92/0.89, and 0.88/0.87, respectively, and there was no significant difference in diagnostic performance between conventional bpMRI and synthetic bpMRI for all readers (p = 0.46, 0.21, and 0.49, for each reader). Furthermore, there was no significant difference in sensitivity, specificity, positive predictive value, and negative predictive value between conventional bpMRI and synthetic bpMRI for both TZ and PZ between the six readers (p = 0.11–0.78).

4.4. Synthetic MRI-based relaxometry measurements for category 3 lesions in PZ

Among the 41 lesions in PZ that were classified by the expert prostate radiologists as PI-RADS category 3, 12 (29.3%), 2 (4.9%), and 27 (65.8%) were pathologically determined to be csPCa, clinically insignificant PCa, and non-cancerous, respectively. Similarly, among the 41 lesions in PZ that were classified by the basic prostate radiologists, 12 (29.3%), 2 (4.9%), and 27 (65.8%) were pathologically determined as csPCa, clinically insignificant PCa, and non-cancerous, respectively. The

Fleiss' kappa values for interobserver agreements regarding relaxometry measurements among expert and basic prostate radiologists were 0.89 and 0.87, respectively. The distribution of relaxometry measurements for csPCa in PZ is shown in Fig. 3. For both expert and basic prostate radiologists, T1-value, T2-value, and PD of csPCa were significantly lower than that of other entities in the PZ ($p < 0.05$). Overall, the combination of T1-value, T2-value, and PD (T1 + T2 + PD) had the highest AUC among all the combinations of relaxometry measurements for csPCa for the PZ: 0.85 for expert prostate radiologists and 0.86 for basic prostate radiologists, respectively.

4.5. Comparison between relaxometry maps derived from synthetic MRI and DCE-MRI PI-RADS scores for category 3 lesions

The sensitivity and specificity of relaxometry measurements from synthetic MRI and DCE-MRI PI-RADS scores for the diagnosis of csPCa in category 3 lesions in PZ are shown in Table 3. For the PZ, the AUCs of T1 + T2 + PD/DCE-MRI PI-RADS score for the diagnosis of csPCa in category 3 lesions were 0.85/0.83 for expert radiologists and 0.86/0.83 for basic radiologists, with no significant difference between T1 + T2 + PD vs. DCE-MRI PI-RADS score for both groups of readers ($p = 0.45$, and 0.29, respectively). Furthermore, there was no significant difference in sensitivity and specificity between T1 + T2 + PD vs. DCE-MRI PI-RADS score for the PZ between the expert and basic groups ($p = 0.35$–1.00).

Table 3
Comparison of the diagnostic performance for csPCa diagnosis between relaxometry measurements from synthetic MRI and the DCE-MRI PI-RADS score for category 3 lesions in PZ according to PI-RADS version 2.1.

Prostate Radiologist	Parameter	Relaxometry maps from synthetic MRI	DCE-MRI PI-RADS score	*p*-value
Expert	Sensitivity, %	83.3	83.3	1.00
	Specificity, %	79.3	82.8	0.48
Basic	Sensitivity, %	83.3	83.3	1.00
	Specificity, %	78.8	81.8	0.35

csPCa: clinically significant prostate cancer; MRI: magnetic resonance imaging; DCE: dynamic contrast-enhanced; PI-RADS: Prostate Imaging Reporting and Data System; PZ: peripheral zone
* $p < 0.05$, statistically significant

5. Discussion

We investigated the feasibility of bpMRI with relaxometry maps using synthetic MRI for primary PCa evaluation. We demonstrated that the diagnostic performance of synthetic bpMRI was comparable to that of conventional bpMRI for primary PCa evaluation in both TZ and PZ, for both expert and basic prostate radiologists. Additionally, the diagnostic performance of bpMRI observed in this study showed a comparable though slightly better diagnostic performance than that was reported in a recent meta-analysis by Cuocolo, et al. (AUC, 0.84) [30] and matches the results of a recent meta-analysis by Woo, et al. on the diagnostic accuracy of mpMRI for PCa (AUC, 0.90) [12]. Furthermore, the sensitivity and specificity of relaxometry maps from synthetic MRI were similar to those of the DCE-MRI PI-RADS scores for the diagnosis of csPCa in PI-RADS category 3 lesions in the PZ, for both expert and basic prostate radiologists. Therefore, the potential weaknesses of bpMRI evaluation, where the diagnostic performance is inferior to that of mpMRI for non-expert radiologists [13,14], and the sensitivity values of bpMRI are lower than those of mpMRI when using the PI-RADS v2.1 system for category 3 lesions [9,15], may be mitigated by combining (synthetic) bpMRI with relaxometry maps. As such, synthetic MRI has a potential as a non-contrast-enhanced method for primary PCa evaluation.

Synthetic MRI, which is an emerging MRI acquisition technique, requires no additional image acquisition time for generating any arbitrary image contrasts after MRI acquisition, and does not require the use

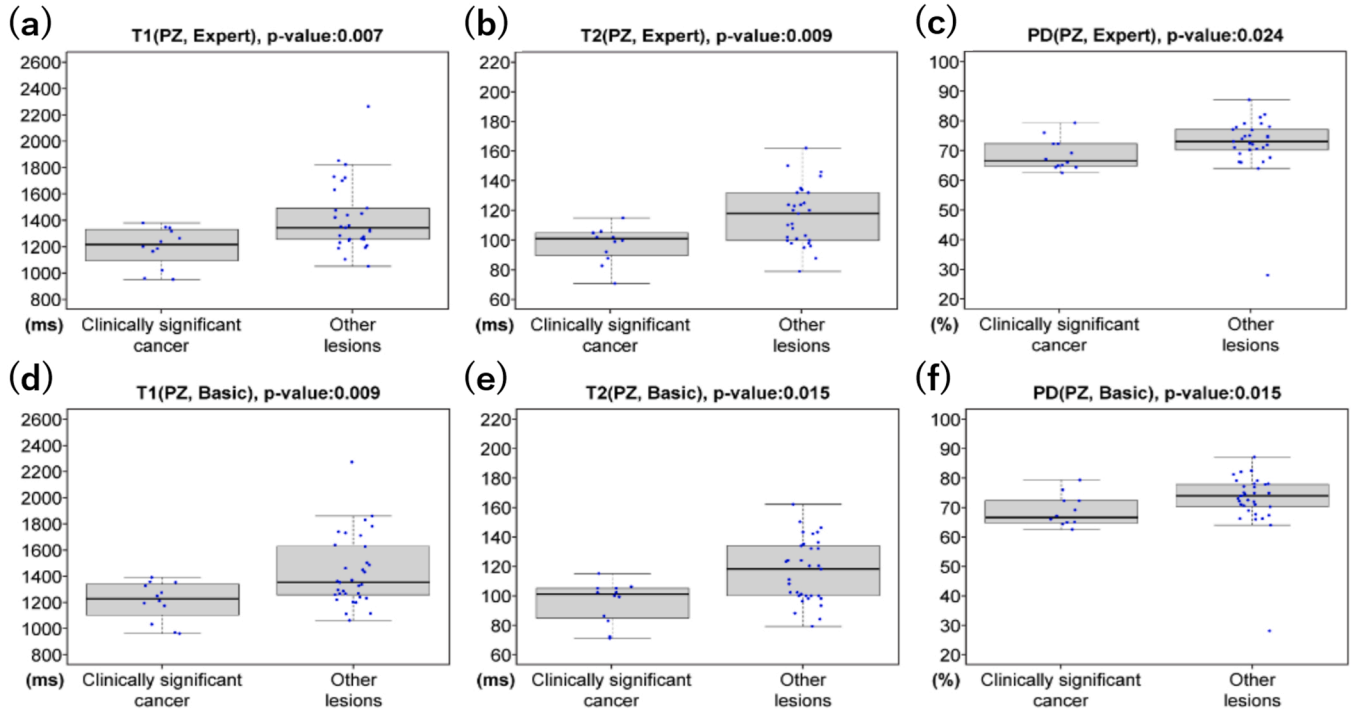

Fig. 3. Boxplots of relaxometry measurements for csPCa and other lesions in PZ. (a)-(f) The T1-value, T2-value, and PD for csPCa were significantly lower than those for other category 3 entities (i.e. clinically insignificant PCa, and non-cancerous) for both expert and basic prostate radiologists ($p < 0.05$). Abbreviations: csPCa: clinically significant prostate cancer; PD: proton density; PZ: peripheral zone. *$p < 0.05$, statistically significant.

of any contrast agents [15–18]. According to a recent report by Hagiwara et al., double inversion recovery images without contrast agents derived from synthetic MRI enabled detection of more plaques in multiple sclerosis patients than conventional double inversion recovery images from dedicated brain MRI within a comparable acquisition time [31]. Moreover, according to a recent report by Yi et al., conventional knee MRI and synthetic MRI showed a substantial-to-almost perfect degree of agreement for the assessment of internal derangement of knee joints [32]. In the image quality analysis of our study, all subjective quality measures analysed (contraction artefacts, motion artefacts, and overall image quality) were comparable between synthetic bpMRI and conventional bpMRI. As indicated in previous studies, the diagnostic performance of bpMRI is inferior to that of mpMRI when interpreted by non-expert radiologists [13,14]. However, as shown in the results of this study, the diagnostic performance of synthetic bpMRI for basic prostate radiologists was similar to that for expert prostate radiologists for primary PCa diagnosis. Therefore, incorporating synthetic MRI into standard clinical PCa screening protocols may be useful, even for basic prostate radiologists.

Previously published literature about relaxometry MRI methods particularly focused on the T2-value for tissue characterisation and has shown that the T2-value of PCa, which has been recognised as a quantitative biomarker reflecting the mobile water content in different tissues, was significantly lower in csPCa than in non-cancerous lesions [33]. However, according to a recent report by Panda et al., the T1-value for category 3 csPCa is also lower than that for non-cancer in the TZ [26]. Our results confirm that both T1-value and T2-value, as quantitatively measured using synthetic MRI, are useful for the discrimination of csPCa from other (benign) entities in PZ. Moreover, as shown in the results of our study, T1 + T2 + PD yielded the highest AUCs. According to the report by Panda et al., the AUC of the combination of T1-value and ADC was 0.81 [26]. Our results (based on T1 + T2 + PD with AUCs of 0.85–0.91) were slightly better than the diagnostic performance metrics published previously.

From a clinical point of view, there are several potential advantages of using synthetic MRI for PCa diagnosis. First, synthetic MRI is a potentially time-saving method due to its relatively shorter examination time; however, if the scan fails, the entire scan has to be repeated, instead of only repeating a single sequence as in conventional MRI [10,16–18]. However, the latter did not occur in any of the patients in our study. It also avoids exposure of patients to the potential risks of gadolinium-based contrast agents (i.e., nephrogenic systematic fibrosis and gadolinium deposition in the brain) [34–36]. Synthetic MRI also nullifies the risk of allergic reactions to contrast agents.

5.1. Limitations

Our study has several limitations. First, we divided the prostate into four regions, and only the index lesion with the highest pathological grade group or size was analysed in patients with multiple lesions, which might have resulted in selection bias. Nevertheless, the concept of the index lesion has been widely used in previous studies, including studies on PI-RADS [8,9,23,24]. Second, MRGB was used as the reference standard in several patients. Histological–radiological correlation is a great challenge in prostate MRI research. In this study, the radical prostatectomy result was used as the final pathological reference standard to minimise histological–radiological mismatch in patients who underwent both MRGB and subsequent radical prostatectomy. The concept of this type of reference standard (radical prostatectomy or MRGB) has been widely used in previous studies, including research on PI-RADS [15,21–23,27,28]. Third, even if MRI findings were negative, we performed a biopsy based on an elevated serum prostate-specific antigen level or abnormal digital rectal examination, which might have caused some selection bias. Fourth, slice thickness of all sequences should be $\leq$ 3 mm (the current study employed a 3.4-mm slice thickness). Fifth, this study was conducted to compare relaxometry measurements from synthetic MRI and the DCE-MRI PI-RADS score for csPCa diagnosis in category 3 lesions according to the literature of PI-RADS v2.1 guideline, while a comparison between these two tests in all lesions (i.e., not only category 3 lesions) was not included in this study. However, for both expert and basic prostate radiologists, the specificity of relaxometry measurements tended to be slightly lower than that of DCE-MRI in the evaluation of category 3 lesions. This trend may also be present in other lesions than only those in category 3. Future studies with larger sample sizes should assess if the diagnostic performance is comparable between relaxometry measurements and the DCE-MRI PI-RADS score in the evaluation of all lesions. Lastly, this prospective single-centre study comprised a relatively small sample size. Further larger, multicentre validation studies are necessary to confirm the results of this study.

6. Conclusions

In conclusion, the diagnostic performance of synthetic bpMRI was comparable to that of conventional bpMRI for primary PCa evaluation. Moreover, the diagnostic performance of relaxometry maps from synthetic MRI was similar to that of DCE-MRI PI-RADS score for csPCa in PI-RADS category 3 lesions in PZ, for both expert and basic prostate radiologists. Therefore, bpMRI with relaxometry maps derived from synthetic MRI shows potential as a contrast agent-free method for primary PCa evaluation.

Ethical Approval

Institutional Review Board approval was obtained.

Funding

This research did not receive any specific grant from funding agencies in the public, commercial, or not-for-profit sectors.

CRediT authorship contribution statement

Yuki Arita: Investigation, Writing – original draft; **Hirotaka Akita:** Resources, Data curation; **Hirokazu Fujiwara:** Resources, Data curation; **Masahiro Hashimoto:** Resources, Data curation; **Keisuke Shigeta:** Resources, Data curation; **Thomas C. Kwee:** Writing – review & editing; **Soichiro Yoshida:** Writing – review & editing; **Takeo Kosaka:** Resources, Data curation; **Shigeo Okuda:** Resources, Data curation; **Mototsugu Oya:** Supervision, Project administration; **Masahiro Jinzaki:** Supervision, Project administration.

Declaration of Competing Interest

The authors declare that they have no known competing financial interests or personal relationships that could have appeared to influence the work reported in this paper.

Acknowledgements

The authors thank Mr. Koshi Okabe and Ms. Sari Motomatsu for their help with data collection.

Appendix A. Supporting information

Supplementary data associated with this article can be found in the online version at doi:10.1016/j.ejro.2022.100403.

References

[1] K.D. Miller, L. Nogueira, A.B. Mariotto, J.H. Rowland, K.R. Yabroff, C.M. Alfano, A. Jemal, J.L. Kramer, R.L. Siegel, Cancer treatment and survivorship statistics, CA Cancer J. Clin. 69 (2019) 363–385, https://doi.org/10.3322/caac.21565.

[2] P.A. Humphrey, Gleason grading and prognostic factors in carcinoma of the prostate, Mod. Pathol. 17 (2004) 292–306, https://doi.org/10.1038/modpathol.3800054.

[3] M.G. Sanda, J.A. Cadeddu, E. Kirkby, R.C. Chen, T. Crispino, J. Fontanarosa, S. J. Freedland, K. Greene, L.H. Klotz, D.V. Makarov, J.B. Nelson, G. Rodrigues, H. M. Sandler, M.E. Taplin, J.R. Treadwell, Clinically localized prostate cancer: AUA/ASTRO/SUO guideline. Part I: risk stratification, shared decision making, and care options, J. Urol. 199 (2018) 683–690, https://doi.org/10.1016/j.juro.2017.11.095.

[4] S. Verma, P.L. Choyke, S.C. Eberhardt, A. Oto, C.M. Tempany, B. Turkbey, A. B. Rosenkrantz, The current state of MR imaging-targeted biopsy techniques for detection of prostate cancer, Radiology 285 (2017) 343–356, https://doi.org/10.1148/radiol.2017161684.

[5] A.B. Rosenkrantz, S. Verma, P. Choyke, S.C. Eberhardt, S.E. Eggener, K. Gaitonde, M.A. Haider, D.J. Margolis, L.S. Marks, P. Pinto, G.A. Sonn, S.S. Taneja, Prostate magnetic resonance imaging and magnetic resonance imaging targeted biopsy in patients with a prior negative biopsy: a consensus statement by AUA and SAR, J. Urol. 196 (2016) 1613–1618, https://doi.org/10.1016/j.juro.2016.06.079.

[6] T.W. Scheenen, A.B. Rosenkrantz, M.A. Haider, J.J. Fütterer, Multiparametric magnetic resonance imaging in prostate cancer management: current status and future perspectives, Investig. Radiol. 50 (2015) 594–600, https://doi.org/10.1097/RLI.0000000000000163.

[7] S. Hattori, T. Kosaka, R. Mizuno, K. Kanao, A. Miyajima, Y. Yasumizu, S. Yazawa, H. Nagata, E. Kikuchi, S. Mikami, M. Jinzaki, K. Nakagawa, A. Tanimoto, M. Oya, Prognostic value of preoperative multiparametric magnetic resonance imaging (MRI) for predicting biochemical recurrence after radical prostatectomy, BJU Int. 113 (2014) 741–747, https://doi.org/10.1111/bju.12329.

[8] J.C. Weinreb, J.O. Barentsz, P.L. Choyke, F. Cornud, M.A. Haider, K.J. Macura, D. Margolis, M.D. Schnall, F. Shtern, C.M. Tempany, H.C. Thoeny, S. Verma, PI-RADS prostate imaging-reporting and data system: 2015, version 2, Eur. Urol. 69 (2016) 16–40, https://doi.org/10.1016/j.eururo.2015.08.052.

[9] B. Turkbey, A.B. Rosenkrantz, M.A. Haider, A.R. Padhani, G. Villiers, K.J. Macura, C.M. Tempany, P.L. Choyke, F. Cornud, D.J. Margolis, H.C. Thoeny, S. Verma, J. Barentsz, J.C. Weinreb, Prostate imaging reporting and data system version 2.1: 2019 update of prostate imaging reporting and data system version 2, Eur. Urol. 76 (2019) 340–351, https://doi.org/10.1016/j.eururo.2019.02.033.

[10] C.K. Kuhl, R. Bruhn, N. Krämer, S. Nebelung, A. Heidenreich, S. Schrading, Abbreviated biparametric prostate MR imaging in men with elevated prostate-specific antigen, Radiology 285 (2017) 493–505, https://doi.org/10.1148/radiol.2017170129.

[11] C.G. Wei, T. Chen, Y.Y. Zhang, P. Pan, G.C. Dai, H.C. Yu, S. Yang, Z. Jiang, J. Tu, Z. H. Lu, J.K. Shen, W.L. Zhao, Biparametric prostate MRI and clinical indicators predict clinically significant prostate cancer in men with “gray zone” PSA levels, Eur. J. Radiol. 127 (2020), 108977, https://doi.org/10.1016/j.ejrad.2020.108977.

[12] S. Woo, C.H. Suh, S.Y. Kim, J.Y. Cho, S.H. Kim, M.H. Moon, Head-to-head comparison between biparametric and multiparametric MRI for the diagnosis of prostate cancer: a systematic review and meta-analysis, AJR Am. J. Roentgenol. 211 (2018) W226–W241, https://doi.org/10.2214/AJR.18.19880.

[13] M. de Rooij, B. Israël, M. Tummers, H.U. Ahmed, T. Barrett, F. Giganti, B. Hamm, V. Logager, A. Padhani, V. Panebianco, P. Puech, J. Richenberg, O. Rouviere, G. Salomon, I. Schoots, J. Veltman, G. Villeirs, J. Walz, J.O. Barentsz, ESUR/ESUI consensus statements on multi-parametric MRI for the detection of clinically significant prostate cancer: quality requirements for image acquisition, interpretation and radiologists’ training, Eur. Radiol. 30 (2020) 5404–5416, https://doi.org/10.1007/s00330-020-06929-z.

[14] M. Gatti, R. Faletti, G. Calleris, J. Giglio, C. Berzovini, F. Gentile, G. Marra, F. Misischi, L. Molinaro, L. Bergamasco, P. Gontero, M. Papotti, P. Fonio, Prostate cancer detection with biparametric magnetic resonance imaging (bpMRI) by readers with different experience: performance and comparison with multiparametric (mpMRI), Abdom. Radiol. 44 (2019) 1883–1893, https://doi.org/10.1007/s00261-019-01934-3.

[15] T. Tamada, A. Kido, A. Yamamoto, M. Takeuchi, Y. Miyaji, T. Moriyo, T. Sone, Comparison of biparametric and multiparametric MRI for clinically significant prostate cancer detection with PI-RADS version 2.1, J. Magn. Reson. Imaging 53 (2021) 283–291, https://doi.org/10.1002/jmri.27283.

[16] J.B. Warntjes, O.D. Leinhard, J. West, P. Lundberg, Rapid magnetic resonance quantification on the brain: optimization for clinical usage, Magn. Reson. Med. 60 (2008) 320–329, https://doi.org/10.1002/mrm.21635.

[17] A. Hagiwara, M. Warntjes, M. Hori, C. Andica, M. Nakazawa, K.K. Kumamaru, O. Abe, S. Aoki, SyMRI of the brain: rapid quantification of relaxation rates and proton density, with synthetic MRI, automatic brain segmentation, and myelin measurement, Investig. Radiol. 52 (2017) 647–657, https://doi.org/10.1097/RLI.0000000000000365.

[18] I. Blystad, J.B.M. Warntjes, O. Smedby, A.M. Landtblom, P. Lundberg, E. M. Larsson, Synthetic MRI of the brain in a clinical setting, Acta Radiol. 53 (2012) 1158–1163, https://doi.org/10.1258/ar.2012.120195.

[19] Y. Arita, T. Takahara, S. Yoshida, T.C. Kwee, S. Yajima, C. Ishii, R. Ishii, S. Okuda, M. Jinzaki, Y. Fujii, Quantitative assessment of bone metastasis in prostate cancer using synthetic magnetic resonance imaging, Investig. Radiol. 54 (2019) 638–644, https://doi.org/10.1097/RLI.0000000000000579.

[20] N. Schieda, C.S. Lim, F. Zabihollahy, J. Abreu-Gomez, S. Krishna, S. Woo, G. Melkus, E. Ukwatta, B. Turkbey, Quantitative prostate MRI, J. Magn. Reson. Imaging 53 (2021) 1632–1645, https://doi.org/10.1002/jmri.27191.

[21] Y. Cui, S. Han, M. Liu, P.-Y. Wu, W. Zhang, J. Zhang, C. Li, M. Chen, Diagnosis and grading of prostate cancer by relaxation maps from synthetic MRI, J. Magn. Reson. Imaging 52 (2020) 552–564, https://doi.org/10.1002/jmri.27075.

[22] A.B. Rosenkrantz, H. Chandarana, N. Hindman, F.-M. Deng, J.S. Babb, S.S. Taneja, C. Geppert, Computed diffusion-weighted imaging of the prostate at 3T: impact on image quality and tumour detection, Eur. Radiol. 23 (2013) 3170–3177, https://doi.org/10.1007/s00330-013-2917-8.

[23] Y. Arita, S. Yoshida, Y. Waseda, T. Takahara, C. Ishii, R. Ueda, T.C. Kwee, K. Miyahira, R. Ishii, S. Okuda, M. Jinzaki, Y. Fujii, Diagnostic value of computed high b-value whole-body diffusion-weighted imaging for primary prostate cancer, Eur. J. Radiol. 137 (2021), 109581, https://doi.org/10.1016/j.ejrad.2021.109581.

[24] F. Giganti, V. Kasivisvanathan, A. Kirkham, S. Punwani, M. Emberton, C.M. Moore, C. Allen, Prostate MRI quality: a critical review of the last 5 years and the role of the PI-QUAL score, Br. J. Radiol. 94 (2021), 20210415, https://doi.org/10.1259/bjr.20210415.

[25] M. Meier-Schroers, C. Marx, F.C. Schmeel, K. Wolter, J. Gieseke, W. Block, A. M. Sprinkart, F. Traeber, W. Willinek, H.H. Schild, G.M. Kukuk, Revised PROPELLER for T2-weighted imaging of the prostate at 3 Tesla: impact on lesion detection and PI-RADS classification, Eur. Radiol. 28 (2018) 24–30, https://doi.org/10.1007/s00330-017-4949-y.

[26] A. Panda, V.C. Obmann, W.-C. Lo, S. Margevicius, Y. Jiang, M. Schluchter, I. J. Patel, D. Nakamoto, C. Badve, M.A. Griswold, I. Jaeger, L.E. Ponsky, V. Gulani, MR fingerprinting and ADC mapping for characterization of lesions in the transition zone of the prostate gland, Radiology 292 (2019) 685–694, https://doi.org/10.1148/radiol.2019181705.

[27] S. Verma, P.L. Choyke, S.C. Eberhardt, et al., The current state of MR imaging-targeted biopsy techniques for detection of prostate cancer, Radiology 285 (2017) 343–356, https://doi.org/10.1148/radiol.2017161684.

[28] V. Kasivisvanathan, A.S. Rannikko, M. Borghi, V. Panebianco, L.A. Mynderse, M. H. Vaarala, A. Briganti, L. Budäus, G. Hellawell, R.G. Hindley, M.J. Roobol, S. Eggener, M. Ghei, A. Villers, F. Bladou, G.M. Villeirs, J. Virdi, S. Boxler, G. Robert, P.B. Singh, W. Venderink, B.A. Hadaschik, A. Ruffion, J.C. Hu, D. Margolis, S. Crouzet, L. Klotz, S.S. Taneja, P. Pinto, I. Gill, C. Allen, F. Giganti, A. Freeman, S. Morris, S. Punwani, N.R. Williams, C. Brew-Graves, J. Deeks, Y. Takwoingi, M. Emberton, C.M. Moore, PRECISION Study Group Collaborators, MRI-targeted or standard biopsy for prostate-cancer diagnosis, N. Engl. J. Med. 378 (2018) 1767–1777, https://doi.org/10.1056/NEJMoa1801993.

[29] H.M. Katz, Multivariable analysis: a primer for readers of medical research, Ann. Intern. Med. 15 (2003) 644–650, https://doi.org/10.7326/0003-4819-138-8-200304150-00012.

[30] R. Cuocolo, F. Verde, A. Ponsiglione, et al., Clinically significant prostate cancer detection with biparametric MRI: a systematic review and meta-analysis, AJR Am. J. Roentgenol. 216 (2021) 608–621, https://doi.org/10.2214/AJR.20.23219.

[31] A. Hagiwara, M. Hori, K. Yokoyama, M.Y. Takemura, C. Andica, T. Tabata, K. Kamagata, M. Suzuki, K.K. Kumamaru, M. Nakazawa, N. Takano, H. Kawasaki, N. Hamasaki, A. Kunimatsu, S. Aoki, Synthetic MRI in the detection of multiple sclerosis plaques, AJNR Am. J. Neuroradiol. 38 (2017) 257–263, https://doi.org/10.3174/ajnr.A5012.

[32] J. Yi, Y.H. Lee, H.T. Song, J.S. Suh, Clinical feasibility of synthetic magnetic resonance imaging in the diagnosis of internal derangements of the knee, Korean J. Radiol. 19 (2018) 311–319, https://doi.org/10.3348/kjr.2018.19.2.311.

[33] W. Liu, B. Turkbey, J. Sénégas, S. Remmele, S. Xu, J. Kruecker, M. Bernardo, B. J. Wood, P.A. Pinto, P.L. Choyke, Accelerated T2 mapping for characterization of prostate cancer, Magn. Reson. Med. 65 (2011) 1400–1406, https://doi.org/10.1002/mrm.22874.

[34] M. Ramalho, J. Ramalho, L.M. Burke, R.C. Semelka, Gadolinium retention and toxicity-an update, Adv. Chronic. Kidney Dis. 24 (2017) 138–146, https://doi.org/10.1053/j.ackd.2017.03.004.

[35] T.J. Fraum, D.R. Ludwig, M.R. Bashir, K.J. Fowler, Gadolinium-based contrast agents: a comprehensive risk assessment, J. Magn. Reson. Imaging 46 (2017) 338–353, https://doi.org/10.1002/jmri.25625. Epub 2017 Jan 13.

[36] T. Kanda, M. Matsuda, H. Oba, K. Toyoda, S. Furui, Gadolinium deposition after contrast-enhanced MR imaging, Radiology 277 (2015) 924–925, https://doi.org/10.1148/radiol.2015150697.